7 Mesoarchaean Gold Mineralisation in the Barberton Greenstone Belt: A Review

Andrea Agangi, Axel Hofmann, Benjamin Eickmann, and Johanna Marin-Carbonne

Abstract

The Barberton Greenstone Belt hosts abundant structurally controlled gold mineralisation of Mesoarchaean age. More than 300 gold occurrences have been reported, although most of the gold production so far (>350 tonnes Au) has come from a handful of deposits located along the northern margin of the greenstone belt. Most deposits are hosted by greenschist-facies metasedimentary and metamafic rocks, with the notable exception of the amphibolite-facies rocks at New Consort mine. Mineralisation is associated with quartz–carbonate veins that truncate major compressional structures at the greenstone belt scale. The age of mineralisation is loosely constrained at circa 3080–3030 Ma, based on U–Pb dating of hydrothermal rutile and titanite. In greenschist-facies deposits, the ore assemblage is dominated by pyrite and arsenopyrite, which contain up to thousands of ppm of 'invisible' gold, Ni–As–Sb sulphides and native gold. At New Consort mine, mineralisation includes massive replacement-style ore and vein-hosted or disseminated types. Both structural studies in the field and microstructural observation point to a multistage ore deposition process, which is reflected in the re-activation of brittle to ductile structures and the overprinting of sulphide assemblages. The presence of mass-independently fractionated S isotopes ($\Delta^{33}S$ = –0.6 to +1.0‰) in pyrite from Sheba and Fairview mines suggests that hydrothermal fluids mobilised S from volcanic and sedimentary rocks of the greenstone belt and places constraints on the origin of the Au itself.

Keywords

Archaean • Gold • Mineralisation • Multiple S isotopes • Barberton

A. Agangi (✉) · A. Hofmann
Department of Geology, University of Johannesburg, Johannesburg, South Africa
e-mail: aagangi@uj.ac.za

B. Eickmann
Isotopengeochemie, Universität Tübingen, Tübingen, Germany

J. Marin-Carbonne
Laboratoire Magmas et Volcans, UCA, IRD, CNRS, Université Lyon—UJM, Saint Étienne, France

Present Address:
J. Marin-Carbonne
Faculté des géosciences et de l'environnement, Institut des sciences de la Terre, University of Lausanne, Lausanne, Switzerland

7.1 Introduction

The Palaeoarchaean Barberton Greenstone Belt is host to some of the earliest known Au mineralisation (Anhaeusser 1976, 1986; de Ronde et al. 1991; Dziggel et al. 2010). The mineralisation is structurally controlled and occurs in strongly deformed greenschist- to amphibolite-facies metamorphic rocks. Deciphering mechanisms and timing of mineralisation in the Barberton Greenstone Belt and other Archaean terrains is important for understanding Archaean tectonic and hydrothermal processes (Anhaeusser 1986; Kolb et al. 2015; Sahoo and Venkatesh 2015; Hazarika et al. 2017; Mishra et al. 2017).

Mineralisation in the Barberton Greenstone Belt has significant economic relevance and, since the discovery of gold in this area in 1882, more than 350 tonnes of gold have been extracted (Anhaeusser 1976; Dirks et al. 2009; Pearton and Viljoen 2017). In plan view, the distribution of the main deposits reveals a heterogeneous distribution of gold mineralisation. Despite the fact that more than 300 deposits and prospects are known in the greenstone belt, the bulk of the gold production comes from a handful of mines, namely Fairview, Sheba, New Consort, Agnes and Princeton mines, all located in the northern portion of the greenstone belt near the contact between the Barberton Greenstone Belt and the Kaap Valley and Stentor plutons (Anhaeusser 1976; Ward 1995, 1999; Dirks et al. 2009) (Fig. 7.1). The fluids

A. Kröner and A. Hofmann (eds.), *The Archaean Geology of the Kaapvaal Craton, Southern Africa*, Regional Geology Reviews, https://doi.org/10.1007/978-3-319-78652-0_7

responsible for mineralisation are believed to have been low-salinity and H_2O-CO_2-rich (de Ronde et al. 1992) and, similar to other orogenic gold deposits, Au is interpreted to have been transported as complexes of reduced S such as Au$(HS)_2^-$ and AuHS (Pokrovski et al. 2014). Structural and microtextural evidence convincingly points at multiphase processes of mineralisation (Agangi et al. 2014; Munyai et al. 2011; Dziggel and Kisters 2019).

Some aspects of the genesis of this mineralisation are still controversial, and some of the open questions include the origin of H_2O-CO_2 mineralising fluids and, by inference, the origin of Au itself. Possible sources of fluids and Au include supracrustal lithologies (volcanic and sedimentary rocks), felsic intrusions, and the mantle. The mineralisation is believed to have occurred between circa 3080 and 3030 Ma, based on rutile and titanite U-Pb ages, but precise timing of mineral deposition is also uncertain, given the scarcity of available data (de Ronde et al. 1992; Dziggel et al. 2010; Dirks et al. 2013).

Several reviews have dealt with gold mineralisation in the Barberton Greenstone Belt and have mostly focussed on the meso- to mega-scale structural and metamorphic aspects of various mines (Anhaeusser 1986; Dziggel et al. 2007; Pearton and Viljoen 2017; Dziggel and Kisters 2019). Here, we review some of the main characteristics of gold deposits in the Barberton Greenstone Belt with an emphasis on geochemical and microstructural characteristics. We refer to the mentioned papers for more complete information on the control of structures and deformation on mineralisation. We distinguish mineralisation hosted in mostly greenschist-facies rocks from mineralisation hosted in amphibolite-facies rocks. We then evaluate different models of genetic mechanisms of mineralisation.

7.2 Geological Setting of the Barberton Greenstone Belt

The Palaeoarchaean Barberton Greenstone Belt is situated in the eastern part of the Kaapvaal craton, southern Africa (Fig. 7.1). Its ca. 3550–3220 Ma volcano-sedimentary succession, which forms the Barberton Supergroup (formerly Swaziland Supergroup), is preserved in a southwest-northeast-trending belt surrounded by granitoid rocks belonging to the trondhjemite-tonalite-granodiorite (TTG) and granite-granodiorite-syenogranite (GMS) series (Viljoen and Viljoen 1969; Lowe and Byerly 2007; de Wit et al. 2019). The supracrustal succession has been subdivided into three main lithostratigraphic units: the Onverwacht Group, the Fig Tree Group, and the Moodies Group, in ascending order (SACS 1980).

The Inyoka–Saddleback Fault System, a southwest to northeast-trending structure interpreted by some as a suture zone, separates a northern and a southern terrane of different age and geochemical characteristics (Kamo and Davis 1994; Kisters et al. 2003; Lowe and Byerly 2007). The Onverwacht Group consists mostly of komatiite, komatiitic basalt and basalt, with minor felsic volcanic rocks, and has been dated at circa 3550–3300 Ma in the southern terrane (Kröner et al. 1996, 2016). North of the Inyoka-Saddleback fault, the Onverwacht Group is composed of the Weltevreden Formation, which contains mafic-ultramafic volcanic rocks and numerous layered ultramafic complexes (Anhaeusser 2001; Stiegler et al. 2012). The Fig Tree Group is a largely marine, northwards deepening succession dominated by turbiditic greywackes, shales, banded iron formation and cherts (Lowe 1999; Hofmann 2005). The Moodies Group is a shallow marine to continental succession characterised by coarse-grained clastic sedimentary rocks, mainly sandstones and conglomerates, and only minor shale with a minimum depositional age of 3219 Ma (SACS 1980; Heubeck et al. 2013, 2016; Drabon et al. 2017). The metamorphic grade of the Barberton Greenstone Belt is generally low but increases towards the contacts with the surrounding gneiss domes (Dziggel et al. 2002, 2005; Diener et al. 2005). The structure of the greenstone belt is rather complex and is dominated by steeply plunging synforms separated either by thrust faults or narrow anticlines (Lowe et al. 2012).

The tectonic evolution of the Barberton Greenstone Belt is complex, and the multiple phases of deformation affecting these rocks have been described elsewhere (de Ronde and de Wit 1994; Kamo and Davis 1994; Lowe and Byerly 1999; de Ronde and Kamo 2000; Lana et al. 2010). According to de Ronde and de Wit (1994) and de Ronde and Kamo (2000), four main tectono-metamorphic events affected the greenstone belt. The first of these events (D1) remains to some extent enigmatic. D1 occurred between circa 3445 and 3416 Ma and was restricted to Onverwacht Group rocks in the southern part of the greenstone belt (de Ronde and de Wit 1994). D1 was coeval with the intrusion of TTGs along the southern margin of the greenstone belt and with an early phase of low-pressure amphibolite-facies metamorphism, with estimated peak conditions of ~550 °C and 4.5 kbar (Cutts et al. 2014).

The 3229–3227 Ma D2 event was responsible for the main regional strain and affected the entire greenstone belt (de Ronde and Kamo 2000; Schoene et al. 2008). Event D2 coincided with emplacement of TTG intrusions such as the 3227 Ma Kaap Valley Tonalite, the 3290–3230 Ma Badplaas pluton and the 3236 Ma Nelshoogte pluton (Kamo and Davis 1994; Kisters et al. 2010; Matsumura 2014). During this event, the rocks of the lowermost units of the Onverwacht Group, the Theespruit and Sandspruit Formations, experienced high-pressure amphibolite-facies metamorphism (Dziggel et al. 2002, 2005; Diener et al. 2005; Moyen et al. 2006). D2 marked the switch from sedimentation of the

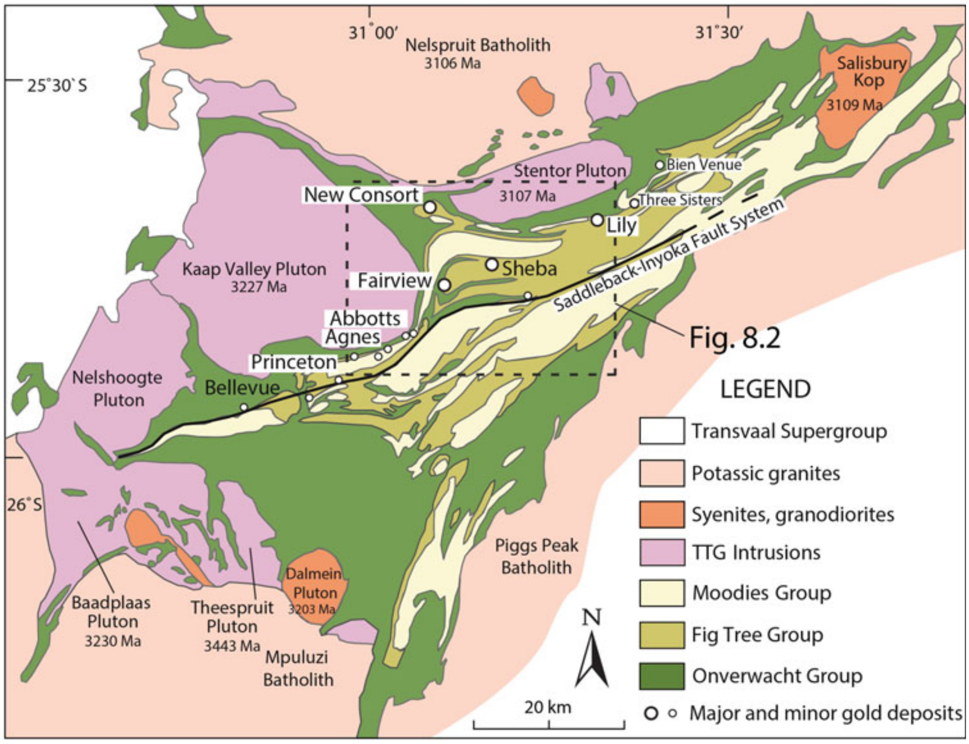

Fig. 7.1 Geological map of the Barberton Greenstone Belt and distribution of the main gold deposits (modified from de Ronde et al. 1992). Dashed line indicates position of Fig. 7.2

3260–3230 Ma Fig Tree Group in a relatively deep marine environment to the ~3225 Ma Moodies Group in a shallow marine to continental environment (de Ronde and de Wit 1994; Kamo and Davis 1994; de Ronde and Kamo 2000; Kisters et al. 2010; Heubeck et al. 2013). The structures associated with D2 are truncated by potassic intrusions such as the 3203 Ma Dalmein pluton in the southern part (Lana et al. 2010), which places constraints on the end of this phase of deformation. The tectonic circumstances that gave rise to the D2 event are controversial and directly mirror the controversy relating to the nature of Archaean tectonics and the origin of TTG magmas. Some authors interpreted D2 as the consequence of compression, subduction and accretion of the southern terrane along the Inyoka-Saddleback Fault during northwards-directed subduction (Moyen et al. 2006; Kisters et al. 2010). In this interpretation, the syntectonic granitoids to the north of the greenstone belt represent the roots of a volcanic arc. D2 was synchronous with, or immediately followed by, a period of syn-orogenic extension and solid-state doming that eventually resulted in the steepening of fabrics during the orogenic collapse of the belt (Kisters et al. 2003). Others interpret this deformation as a result of crustal overturn due to density inversions between buoyant (partially molten) TTG intrusions and cooler, denser greenstones (Anhaeusser 1984; Van Kranendonk et al. 2009). These authors argue that the relatively high-pressure conditions and the low temperature/pressure gradients can be achieved during sagging of the supracrustal succession.

The later, post-D2 events are less clear as geochronological constraints are scarce, and deformation gave rise to reactivation of earlier shear zones. The D3 tectonic event appears to have been related to NW-SE directed compression and orogen-parallel stretching accommodated by strike-slip shear zones (de Ronde and de Wit 1994). D3 structural elements thus parallel those of D2 (de Ronde and de Wit 1994). The timing of D3 has been constrained at <3126 Ma (de Ronde and Kamo 2000), although much looser time constraints (circa 3220–3080 Ma) were inferred for this event by other authors (de Ronde and de Wit 1994; Kamo and Davis 1994; Schoene et al. 2008). The D4 tectonic event was characterised by a switch to transtensional deformation (de Ronde and de Wit 1994). Geochronological constraints on this event are few and suggest that D4 occurred at around ~3080 Ma, based on U-Pb ages on hydrothermal rutile from Fairview mine (de Ronde et al. 1991; de Ronde and de Wit 1994).

Gold mineralisation is interpreted to be associated with D3 and/or D4 deformation stages. The age of ~3080 Ma (de Ronde et al. 1991), estimated on rutile in an altered, although not mineralised, sample offers a good indication of the timing of hydrothermal alteration at Fairview mine. However, much younger ages (3027 Ma) have been obtained from titanite associated with sulphide mineralisation at New Consort mine (Dziggel et al. 2010), and a maximum age of ~3015 Ma was estimated based on the zircon age of a felsic dyke interpreted to be syn- mineralisation at Fairview mine (Dirks et al. 2013).

7.3 Greenschist-Facies Gold Deposits

Gold deposits associated with host rocks at greenschist-facies grade are the most abundant in the Barberton Greenstone Belt and include the well-studied Sheba and Fairview mines. The greenschist-facies deposits all share distinctive alteration characteristics and structural style. Mineralisation is spatially associated with major D2 compressional structures (Figs. 7.1 and 7.2), although mineralising fluids are interpreted to have moved along later, extensional faults that crosscut D2 compressional structures (de Ronde et al. 1991; Dirks et al. 2009, 2013).

Gold mineralisation is hosted by different lithologies, ranging from metamafic–ultramafic rocks of the uppermost Onverwacht Group to metasedimentary rocks (greywacke, shale) of the Fig Tree and Moodies Groups. The Fairview and Sheba mines are located largely south of the Sheba Fault, although both mines exploit ore bodies on the northern side of the fault as well. The Sheba Fault has been interpreted as a north-west verging thrust fault that structurally superposed Fig Tree Group (meta)greywacke and shale of the Ulundi syncline onto Moodies Group arenites of the Eureka syncline (Anhaeusser 1976; Ward 1999; de Ronde and Kamo 2000) (Fig. 7.2). Minor metamafic rocks of the Onverwacht Group are preserved between the Ulundi and Eureka synclines as tight antiformal structures made of talc-carbonate schist of the Zwartkoppie Formation[1] (Schouwstra and De Villiers 1998; Schouwstra 1995).

Mineralisation occurs as auriferous quartz-carbonate ± rutile veins with associated semi-massive replacement sulphide bodies developing as part of wall-rock alteration (Schouwstra 1995). Alteration zones associated with mineralisation in mafic lithologies include, from distal to proximal, talc-carbonate, quartz-carbonate, fuchsite-quartz-carbonate ± sulphides, and fuchsite-quartz-sulphides ± carbonate (Schouwstra 1995). Sericite is present instead of fuchsite as the K-mica in the neighbouring greywacke and shale. Mineralised fractures in the Sheba–Fairview area extend for tens of metres, trending northeast to east-northeast, and are arranged in hundreds of metre-scale fracture zones (Dirks et al. 2009). In microtextural observations, veins directly associated with mineralisation appear as dilatant, mostly brittle structures, as demonstrated by euhedral prismatic quartz growing from the walls inwards (Agangi et al. 2014) (Fig. 7.3a).

The mineralisation occurs within or around quartz-carbonate veins that truncate the foliation (Fig. 7.3b, c). The mineralisation hosted in metapelite and greywacke at Fairview mine is dominated by arsenopyrite and pyrite, with minor chalcopyrite, gersdorffite, galena and Sb-sulphides. Mineralisation hosted in metamafic–ultramafic rocks at Sheba mine is typically dominated by pyrite and also contains As–Ni-sulphides, chalcopyrite, sphalerite and minor galena (Fig. 7.3d). Gold occurs in a variety of forms, as 'invisible' (or refractory) gold in sulphides, as free gold grains in quartz-carbonate veins, and as sulphide-hosted inclusions of native gold (Cabri et al. 1989; de Ronde et al. 1992).

At Sheba and Fairview mines, gold is mostly hosted in arsenopyrite and pyrite, both as micro-inclusions (Fig. 7.3e) and as finely dispersed, sub-microscopic Au (refractory gold). The concentrations and distribution of invisible Au and other trace elements in sulphides have been studied by different methods, including electron microprobe (EPMA), secondary ion mass spectrometry (SIMS) and proton-induced X-ray emission (PIXE) (Cabri et al. 1989; Agangi et al. 2014; Altigani et al. 2016). These studies found that Au concentrations are extremely heterogeneous and vary from <300 ppm (the EPMA detection limit in Cabri et al. 1989 study) to 4400 ppm Au even in a single arsenopyrite grain from Sheba mine, and up to 1020 ppm have been measured in pyrite at Sheba mine. In the Au versus As diagram (Fig. 7.4), pyrite compositions from mineralised samples at Sheba and Fairview mines plot both above and below the Au-saturation line of Reich et al. (2005). This is compatible with the presence of Au in different oxidation states and crystallographic positions, namely Au^+ included in the crystal lattice and Au^0 in gold inclusions. Mapping of trace element distributions at the micrometre scale has highlighted complex intragranular textures that indicate multiple phases of growth, resorption and recrystallisation of sulphide minerals (Fig. 7.5; Cabri et al. 1989; Agangi et al. 2014, 2015).

The largely refractory nature of gold (below the zone of surface oxidation) in these deposits requires the sulphide ore minerals to be oxidised during the process of extraction in order to liberate the gold. In the past, this was achieved by roasting, with consequent production of large amounts of SO_2 gas and volatile As oxides, a process that posed a considerable environmental hazard. Oxidation is now carried out through biogenic means using sulphide-oxidising bacteria, such as Thiobacillus ferrooxidans (Barberton Mines 2010).

7.4 Amphibolite-Facies Gold Deposits—The New Consort Mine

The New Consort mine (Figs. 7.1 and 7.2) represents an exception in the Barberton Greenstone Belt in being one of the few gold deposits hosted in amphibolite-facies rocks. It is located north of Sheba and Fairview mines and occurs in

[1]The Zwartkoppie Formation is not recognised by SACS and its use is informal.

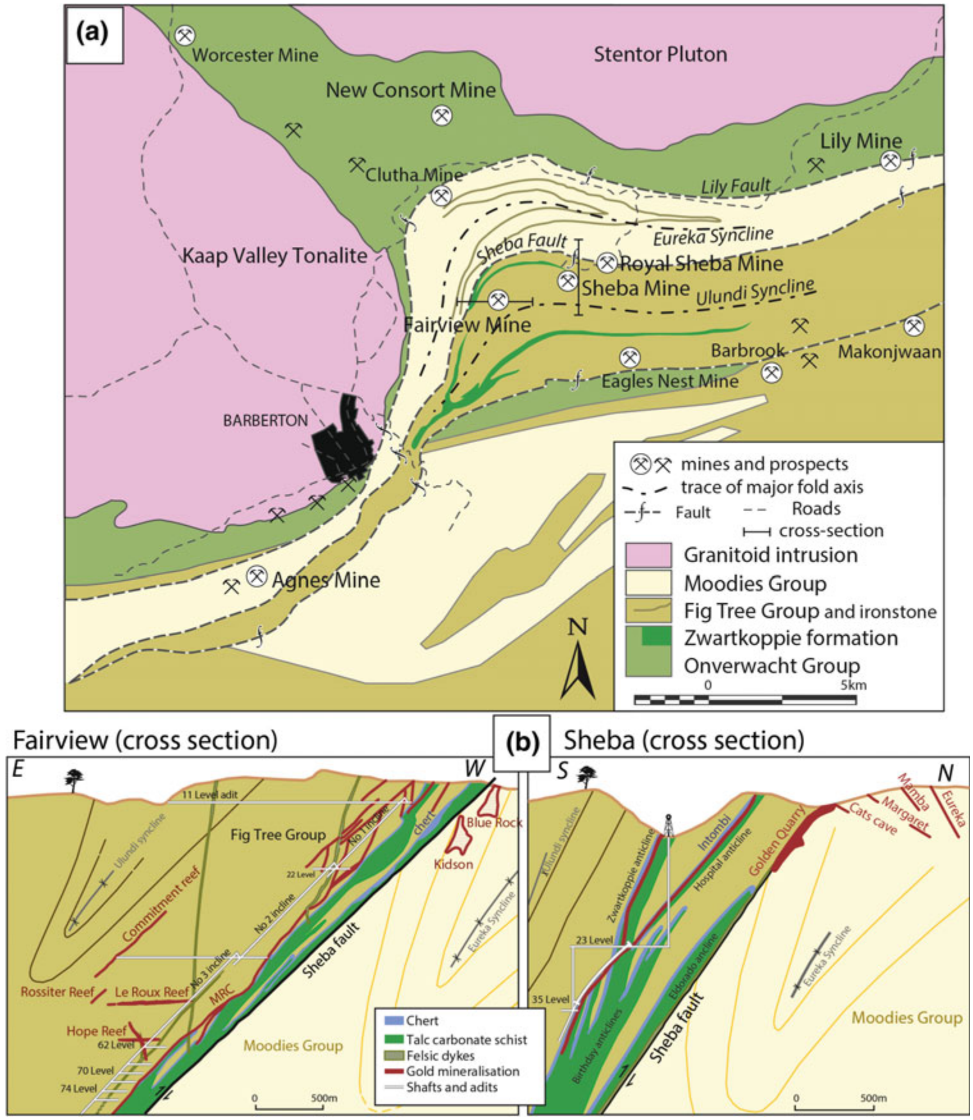

Fig. 7.2 **a** Map of the Eureka and Ulundi synclines and location of gold deposits (modified from Dirks et al. 2009), **b** cross sections of Fairview and Sheba mines (modified from Barberton gold mines 2014)

the hanging wall of the contact between greenstone lithologies and the Stentor Pluton. Mineralisation is hosted by upper greenschist- to upper amphibolite-facies rocks and is associated with the Consort Bar, a mylonitic shear zone separating (ultra)mafic rocks and chert of the Onverwacht Group from clastic sedimentary rocks of the Fig Tree Group (Otto et al. 2007; Munyai et al. 2011). Mineralisation is found in three bodies, the Seven Shaft Shoot, Isaura Shoot, and Prince Consort Shoot. The style of mineralisation in underground workings includes massive replacement-style ore and vein-hosted or disseminated mineralisation (Otto et al. 2007).

Two phases of mineralisation have been identified: the early phase in the footwall, characterised by löellingite-pyrrhotite ore assemblages and a high-temperature alteration calc-silicate assemblage composed of garnet, clinopyroxene, hornblende, K-feldspar, quartz, calcite and biotite (Dziggel et al. 2007; Otto et al. 2007; Dziggel and Kisters 2019). Pressure-temperature estimates for first-phase alteration assemblages in metamafic and intercalated metasedimentary rocks are circa 600–700 °C and 6–8 kbar (Otto et al. 2007).

The second, and main, phase of mineralisation has been attributed to oblique shear zones crosscutting the Consort Bar and was associated with the development of Cr-muscovite-K-feldspar-plagioclase-quartz or Cr-muscovite-tourmaline-plagioclase-rutile as typical alteration assemblages proximal to ore. This second mineralisation event occurred at temperatures ranging from 520 to 600 °C and pressures between 1 and 3 kbar; the ore assemblages vary from arsenopyrite-pyrrhotite to arsenopyrite-pyrrhotite-chalcopyrite-löellingite with increasing depth and temperature (Dziggel et al. 2006, 2010; Otto et al. 2007). Shearing was accompanied by emplacement of pegmatite that has been dated at

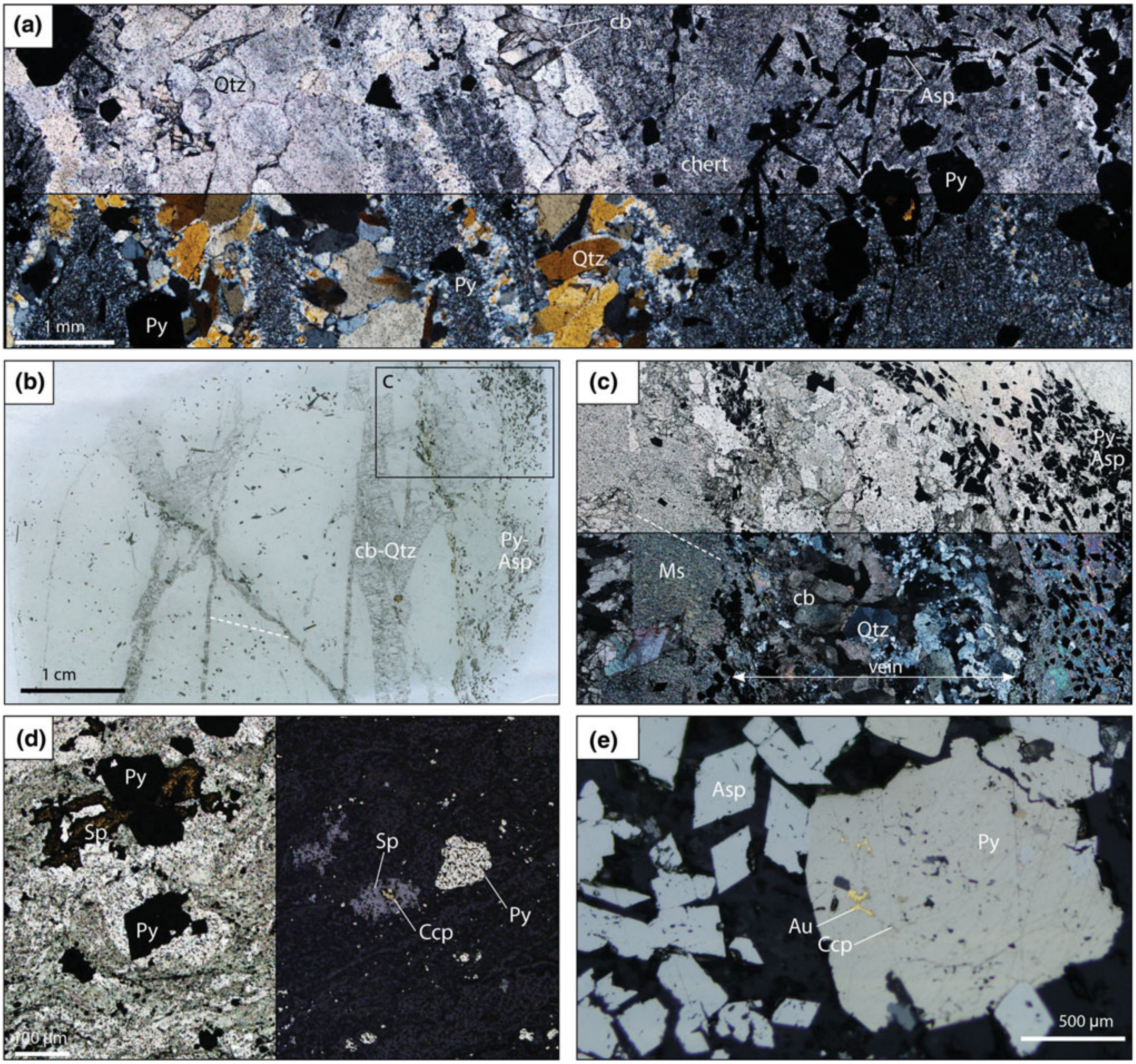

Fig. 7.3 Ore microtextures of samples from Sheba and Fairview mines. **a** Quartz-carbonate vein in chert, Fairview mine. Pyrite and arsenopyrite are present in the host rock. Note quartz crystals growing perpendicular to the vein walls, indicating dilatant behaviour of the cracks. **b**, **c** Carbonate-quartz veins in metagreywacke at Fairview mine. Arsenopyrite and pyrite are visible in both the vein and the alteration halo. Foliation is indicated by dashed lines. **d** Pyrite, sphalerite and chalcopyrite in metamafic schist at Sheba mine. **e** Pyrite-arsenopyrite ore with micro-inclusions of native gold and chalcopyrite, Fairview mine. All images transmitted polarised light, except for **a** and **c** (crossed polarisers in lower half), **d** (reflected light in right-hand half) and **e** (reflected light). Abbreviations: Asp arsenopyrite, cb carbonate, Ccp chalcopyrite, Ms K-mica, Py pyrite, Qtz quartz, Sp sphalerite

3040 ± 84 Ma (Rb–Sr whole-rock; Harris et al. 1995). Overall, textural relations and thermometric estimates indicate a clock-wise P-T path with a near-isobaric decompression to 520–600 °C and 1–3 kbar followed by near-isobaric cooling (Dziggel et al. 2006).

Munyai et al. (2011) and Dirks et al. (2013) focussed their observations on gold-associated fractures on surface exposure at, and in the vicinity of, New Consort mine. In stark contrast with what has been described earlier, they described gold mineralisation associated with low-temperature alteration assemblages and brittle deformation that developed during late-stage extensional tectonics. Thus, mineralisation at New Consort mine and surrounding areas is multiphase and may have formed at very different temperature conditions at different times (Dziggel and Kisters 2019).

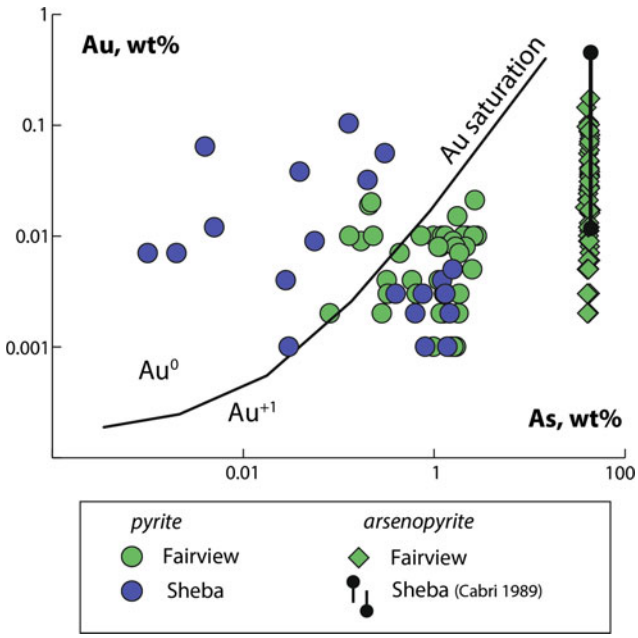

Fig. 7.4 Plot of Au versus As content of pyrite and arsenopyrite grains from Fairview and Sheba mines (data from Agangi et al. 2014 and Cabri et al. 1989). Gold saturation line in arsenian pyrite from Reich et al. (2005)

7.5 Fluid Inclusion and Mineral Stable Isotope Compositions

Fluid inclusion studies from the major deposits indicate low-salinity (NaCl eq = 5–6 wt%), H_2O-CO_2-rich fluids, and homogenisation temperatures in the T = 290 to 310 °C range (de Ronde et al. 1992). As-in-arsenopyrite geothermometry at Fairview mine indicates temperatures between <300 and 400 °C (Agangi et al. 2014). These temperature estimates are in broad agreement with the greenschist-facies alteration assemblages. Based on O, H and C isotope analyses of mineralisation-related quartz and carbonate, the ore fluid would have had narrow ranges of δ^{18}O (+4.7 to + 5.8‰), δ^{13}C (−4.5 to −2‰) and δD (−35 to −41‰), recalculated based on fluid-mineral equilibria at 300 °C (de Ronde et al. 1992). Hydrothermal sulphides have slightly positive δ^{34}S values (+1.2 to +3.9‰) for pyrite and arsenopyrite (Kakegawa and Ohmoto 1999). Overall, the fluid inclusion compositions and mineral stable isotope values indicate distinct homogeneity of mineralising fluids at the greenstone belt scale.

Despite the complexity of sulphide textures and trace element compositions, δ^{34}S values are confined to a narrow range of moderately positive values (de Ronde et al. 1992; Kakegawa and Ohmoto 1999) which limits the use of S isotopes as tracers of the fluid source. As a further complication, δ^{34}S values are affected by a complex range of processes during S transport and precipitation and associated redox reactions that can have overlapping effects. However, recent developments in S isotope studies have revealed that sulphate and sulphide minerals in the Archaean and early Palaeoproterozoic bear mass-independently fractionated S isotopes (MIF-S, indicated by the notation $\Delta^{33}S = \delta^{33}S - 0.515 \cdot \delta^{34}S$) (Farquhar et al. 2000; Ono et al. 2003; Johnston 2011). MIF-S signals are interpreted to be the footprint of photolytic reactions caused by UV irradiation of S gases (such as SO_2) in an O_2-free Archaean atmosphere, which would produce sulphide with $\Delta^{33}S > 0$ and sulphate with $\Delta^{33}S < 0$. Once produced, MIF-S is very robust and only slightly affected by most mass-dependent fractionation-inducing abiogenic and biogenic processes so that it can be used as a tracer of S processed in the atmosphere.

In situ multiple S isotope analyses of pyrite obtained by ion microprobe (SIMS) from samples of Fairview and Sheba mines revealed MIF-S with Δ^{33}S deviating significantly towards both positive and negative values (Δ^{33}S = −0.6 to +1.0‰) (Agangi et al. 2016). In the Δ^{33}S versus δ^{34}S plot, these values match the distribution peak of S compositions of pyrite and whole-rock analyses of the entire volcano-sedimentary succession and suggest derivation of S from the Barberton Supergroup (Fig. 7.6). Given the variability in Δ^{33}S, S may have been scavenged from different rock types and then been transported by hydrothermal fluids responsible for Au mineralisation. More specifically, negative Δ^{33}S values have been measured in sulphides from volcanic-hosted massive sulphide deposits (VHMS) of the Bien Venue deposit of the Fig Tree Group and hydrothermally altered mafic and ultramafic rocks of the Komati Formation, Onverwacht Group (Montinaro et al. 2015). These rocks are interpreted to have derived their S isotopic signature from interaction with heated seawater and to have inherited the typically negative Δ^{33}S values of Archaean seawater sulphate (Bao et al. 2007; Montinaro et al. 2015). They are thus possible sources of some S (and Au) for the sulphides at Sheba and Fairview mines. Positive Δ^{33}S and δ^{34}S values were measured in pyrite from chert, conglomerate and dolomite from the Onverwacht and Fig Tree Groups, as well as from bulk shales from the Fig Tree Group (Grosch and McLoughlin 2013; Roerdink et al. 2013; Montinaro et al. 2015). In particular, some shale samples and pyrite from barite-free samples show a steep negative $\Delta^{33}S/\delta^{34}S$ slope that resembles the distribution of pyrite analyses at Sheba-Fairview. Irrespective of the origin of this negative trend, which may result from mixing of different S components or represent a primary photolytic signal (Roerdink et al. 2013), the similarity to the values observed for hydrothermal pyrite at Sheba-Fairview mines implies that similar rocks may be a good source of S in the Au deposits (Fig. 7.6b).

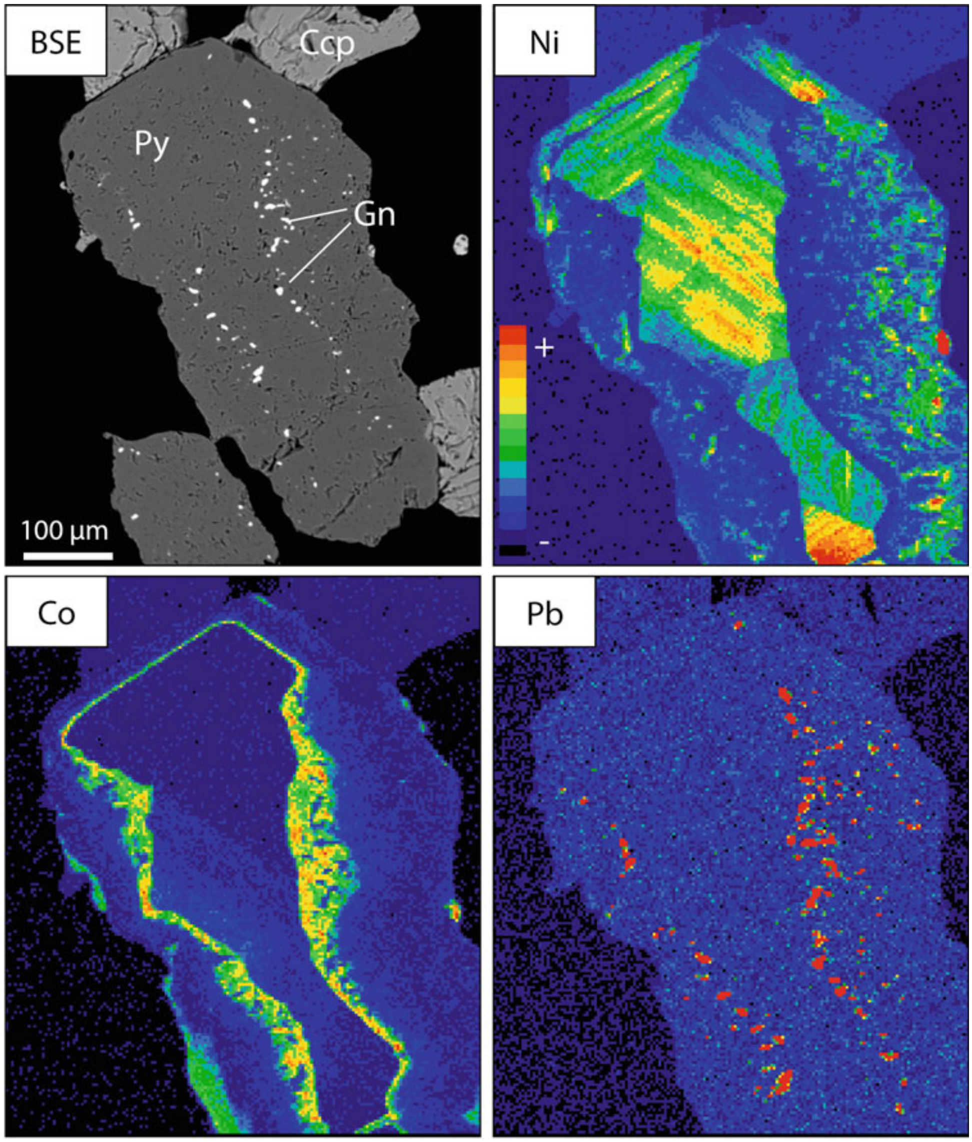

Fig. 7.5 BSE image and Ni-Co-Pb X-ray maps of pyrite from Sheba mine. Abbreviations: Ccp chalcopyrite, Gn galena, Py pyrite

7.6 Discussion and Conclusions

7.6.1 Sources of S, Fluids, and Gold: Internal or External to the Greenstone Belt?

The origin of mineralising fluids and Au in Archaean greenstone belts has proved to be elusive, and the various hypotheses proposed reflect the difficulty in the identification of such sources in structurally-controlled Au deposits, both in Precambrian and Phanerozoic ages (Hronsky et al. 2012; Gaboury 2013; Goldfarb and Groves 2015). Possible sources of sulphur in Archaean orogenic gold deposits include supracrustal rocks (Groves et al. 2003; Phillips and Powell 2009; Tomkins 2013), hydrothermal systems related to felsic magmatism (Salier et al. 2005; Doublier et al. 2014), the lower crust, and the mantle (Hronsky et al. 2012; Fu and Touret 2014).

The hypothesis of a magmatic origin for mineralising fluids has been proposed in several cases of Archaean structurally-controlled Au deposits, such as in Neoarchaean Au deposits of Western Australia, based on the presence of coeval magmatism (Wang et al. 1993; Doublier et al. 2014), trace element signature of accessory minerals (Bath et al. 2013), and Pb and noble gas isotope studies (Qiu and McNaughton 1999; Kendrick et al. 2011). A causal relationship between plutonism and Au mineralisation in the Barberton Greenstone Belt has been proposed mostly based on spatial distribution (Anhaeusser 1976, 1986). In the Barberton Greenstone Belt, mineralisation post-dates the main phase of potassic granite plutonism, which caused the emplacement of extensive batholiths, such as the

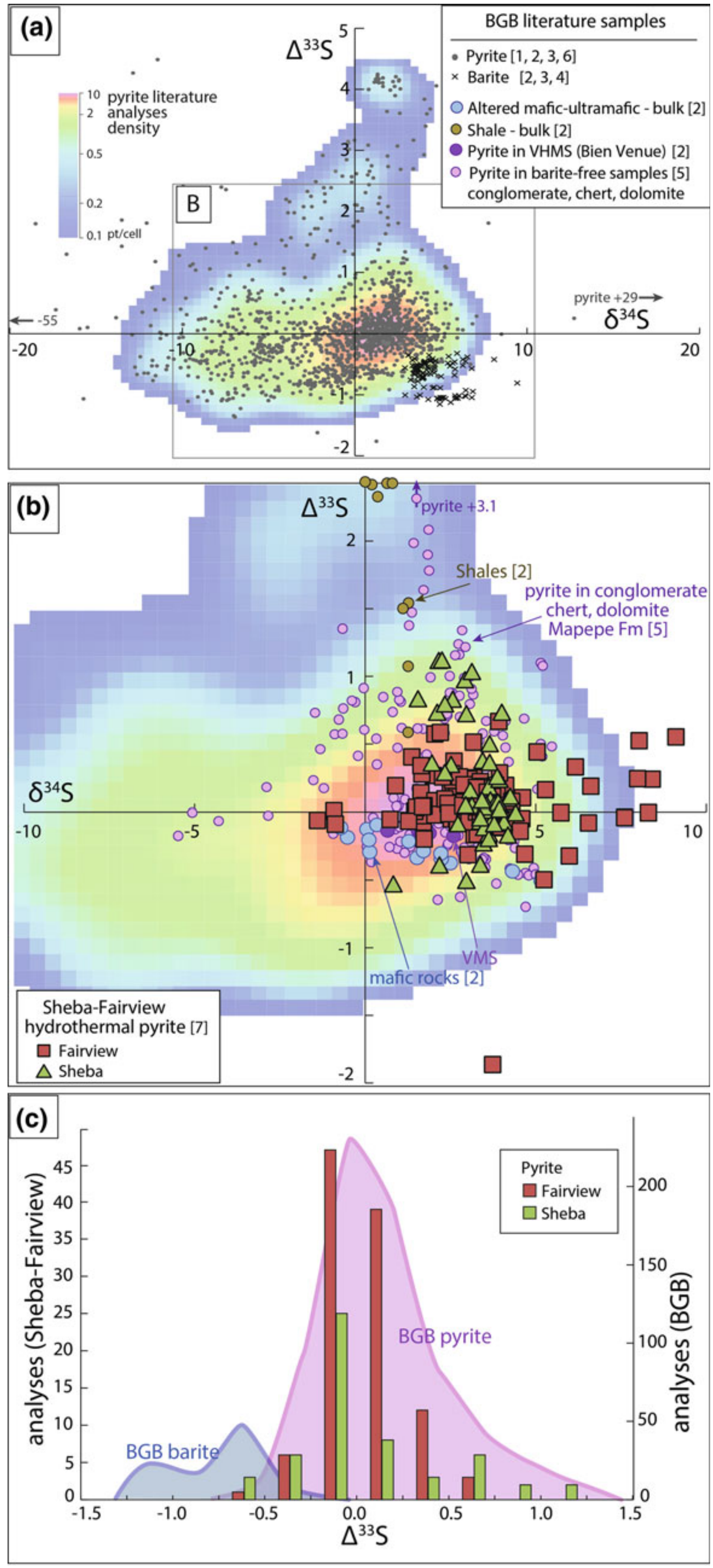

Fig. 7.6 Comparison of S isotope analyses of pyrite associated with gold mineralisation at Sheba and Fairview mines, and pyrite and barite from different units of the Barberton Greenstone Belt. **a** Δ^{33}S versus δ^{34}S plot of pyrite and barite from different units of the Barberton Greenstone Belt (n = 1680) and density distribution of pyrite data. **b** Δ^{33}S versus δ^{34}S plot of pyrite from Au-mineralised samples from Sheba and Fairview mines and some representative rocks of the Barberton Greenstone Belt. **c** Histogram of Δ^{33}S of pyrite from Sheba and Fairview mines compared with Barberton Greenstone Belt pyrite and barite. Data from: (1) Philippot et al. (2012), (2) Montinaro et al. (2015), (3) Roerdink et al. (2012), (4) Bao et al. (2007), (5) Roerdink et al. (2013), (6) Grosch and McLoughlin (2013), (7) Agangi et al. (2016)

3160–3090 Ma Mpuluzi Batholith (Kamo and Davis 1994; Murphy 2015) and the circa 3067 Ma Stentor pluton (Kamo and Davis 1994), and was accompanied by emplacement of small granitic dykes (porphyries) observed in different gold mines. However, the role of these dykes in the mineralising process is not clear. A magmatic source is expected to have $0 \pm 0.2‰$ $\Delta^{33}S$ (Farquhar et al. 2000) so that the MIF-S measured at Sheba and Fairview mines requires the involvement of atmospherically processed S (Fig. 7.6b).

A mantle derivation of CO_2-bearing mineralising fluids has been proposed in recent models that aimed at linking the presence of various types of gold deposits with the presence of "fertile' metasomatised lithospheric mantle (Hronsky et al. 2012; Fu and Touret 2014). This is particularly applicable in the presence of mafic mantle magmas coeval with mineralisation (de Boorder 2012). However, in the Barberton Greenstone Belt magmas coeval with mineralisation are felsic, and the marked MIF-S also argues against such a deep origin of fluids.

Homogeneity of fluid inclusion salinity and elemental compositions (H_2O, CO_2, CH_4), stable isotope compositions of minerals and temperature estimates (in greenschist-facies deposits) suggest a homogeneous source of mineralising fluids at the greenstone belt scale. This source has been identified as external to the Barberton Greenstone Belt (de Ronde et al. 1992). This homogeneity of major element and isotope compositions does not imply constant content of metals, as indicated by zoning of sulphide minerals (Fig. 7.5). Otto et al. (2007) estimated that mineralisation at New Consort mine occurred at peak conditions in the Fig Tree sedimentary rocks forming the hanging wall of the Consort Bar, whereas the Onverwacht Group rocks had already experienced metamorphic peak and were on their retrograde path. They concluded that, as a consequence, the host rocks are unlikely sources of fluids (also see Dziggel and Kisters 2019).

In apparent contrast, multiple S isotope analyses with non-zero MIF-S values imply an atmospheric source, and heterogeneous $\Delta^{33}S$ values suggest that a variety of rocks with different $\Delta^{33}S$ acted as S sources for mineralising fluids. Similar results have been obtained from multiple S isotope analyses of pyrite and pyrrhotite of various Neoarchaean gold deposits of the Yilgarn Craton of Western Australia (Selvaraja et al. 2017). These authors underlined the importance of shales as sources of gold in Archaean structurally controlled gold deposits. A sedimentary rather than igneous source for Barberton gold would be in agreement with low Au contents of komatiites from the Barberton Supergroup (Hofmann et al. 2017).

The microscale heterogeneity of $\Delta^{33}S$ values implies that the ore-forming fluid was isotopically heterogeneous, and variable MIF-S values were not completely homogenised during hydrothermal fluid flow. The isotopic heterogeneity is matched by trace element heterogeneity, which appears as growth zones, recrystallisation domains and veinlets, a characteristic also observed in several other orogenic gold deposits of Archaean and Palaeoproterozoic age (Morey et al. 2008; Fougerouse et al. 2016). This evidence is compatible with a pulsating fluid flow rather than a single large event and suggests that single fluid pulses had a very localised effect in terms of ore deposition. This is similar to what is observed in orogenic gold deposits and typically attributed to periodic fluid pressure build-up and earthquake-related release, also known as fault-valve mechanisms (Sibson et al. 1988).

7.6.2 Timing of Gold Mineralisation in the Barberton Greenstone Belt and Tectonic Context

The age of mineralisation in the Barberton Greenstone Belt is still rather poorly constrained, namely because of a dearth of available data (Fig. 7.7). At Fairview and Sheba mines, porphyry dykes crosscutting mineralisation give good estimates of minimum mineralisation ages. One of these dykes was dated at 3126 Ma (U-Pb on zircon; de Ronde et al. 1991). A rutile separate extracted from a pre-mineralisation, altered dyke at Fairview was dated at 3084 Ma (de Ronde et al. 1992), which may be a good estimate for mineralisation. However, recent U-Pb zircon dating of two mineralised dykes at Golden Quarry, near Sheba mine, has been interpreted to indicate mineralisation at circa 3015 Ma (Dirks et al. 2013). At New Consort mine, a 3027 ± 7 Ma U-Pb age on titanite (Dziggel et al. 2006) associated with main-stage mineralisation and a whole-rock Rb-Sr age of 3040 ± 84 Ma on a syn-mineralisation dyke (Harris et al. 1995) may indicate that mineralisation was caused by a protracted or episodic tectonic activity that lasted for several tens of million years. The multiphase nature of mineralisation at New Consort mine seems to support such a conclusion (Dziggel et al. 2007, 2010; Dziggel and Kisters 2019).

The tectonic regime in operation in the Kaapvaal craton at the time of Au mineralisation are inferred from a fragmentary record, and a complete picture has still to emerge. At the craton scale, mineralisation occurred shortly after the final consolidation of the Kaapvaal craton and at the beginning of an extension phase that led to bimodal volcanism at circa 3074 Ma (Dominion Group, Armstrong et al. 1991) in the central part of the craton and at 2980 Ma to the southeast (Nsuze Group, Hegner et al. 1984).

In the eastern part of the craton, felsic magmatism is indicated by emplacement of the Sinceni granite in Swaziland at circa 3070 Ma (Maphalala and Kröner 1993). A continent-wide felsic magmatic event at circa 3070 Ma is indicated by the abundance of detrital zircons of this age in

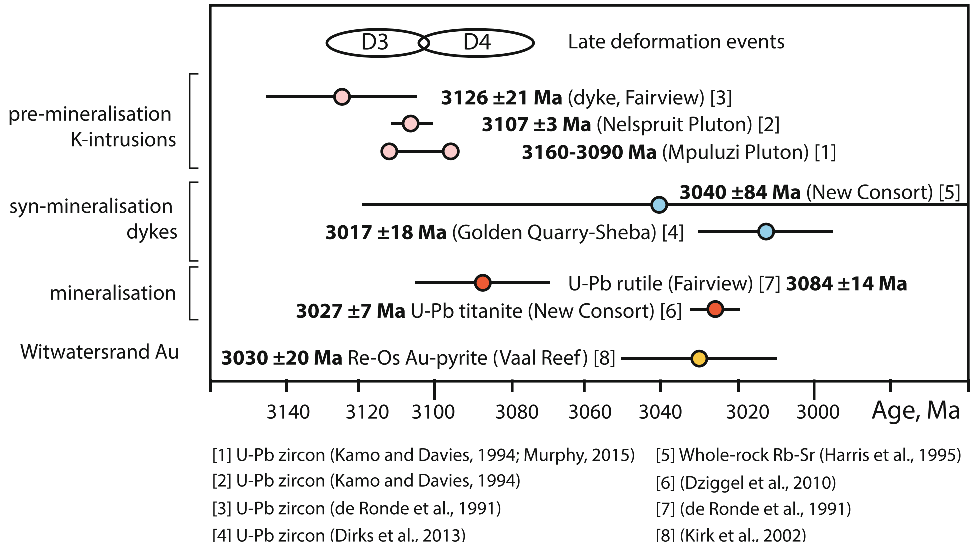

Fig. 7.7 Age constraints on Au mineralisation in the Barberton Greenstone Belt

the Witwatersrand and Pongola Supergroups (Kositcin and Krapez 2004; Wilson and Zeh 2019). At the same time in the north of the Kaapvaal craton, volcanic rocks and sedimentary rocks of the Murchison Greenstone Belt, such as the Weigel Formation and MacKop conglomerate, were deposited, possibly starting from circa 3090 Ma in what is interpreted as a convergent setting (Poujol et al. 1996). Following this magmatic event, volcanic rocks of the Rubbervale Formation in the Murchison Greenstone Belt and Rooiwater granitoids were emplaced at circa 2970 Ma. The emplacement of these volcanic rocks is taken as evidence of crust formation in an arc environment related to the accretion of the northern part of the Kaapvaal craton, the Pietersburg block, to the Witwatersrand block and collision at that time (Zeh et al. 2013).

Gold mineralisation in the Barberton Greenstone Belt is coeval with the tectono-magmatic event related to an extension that shortly followed the final phase of stabilisation of the central Kaapvaal craton. Greenstone gold mineralisation is frequently associated with the latest stage of stabilisation of cratons and can be related to the switch between compression-collision and extensions, when high-angle extensional faults allow deep fluids to flow across the crust (Goldfarb and Groves 2015; Groves et al. 2000). Intriguingly, the available ages for mineralisation partly overlap with Re–Os age determinations of gold and detrital pyrite grains from the Vaal Reef of the Witwatersrand basin (circa 3030 ± 20 Ma, Kirk et al. 2002), the largest gold deposit in the world (Frimmel this volume). Based on this age and an unradiogenic initial $^{187}Os/^{188}Os$ ratio of 0.109, Kirk et al. (2002) concluded that the Witwatersrand gold was eroded from a mantle-derived mafic-ultramafic source rock, although the specific origin of this detrital gold could not be identified. Therefore, gold mineralisation preserved in the Barberton Greenstone Belt may have formed as part of this major crust- and Au-forming event, of which it would represent but a remnant.

Acknowledgements This research was funded by SIEF (Science and Industry Endowment Fund), the NRF (National Research Foundation of South Africa), and the DST-NRF Centre of Excellence for Integrated Mineral and Energy Resource Analysis (CIMERA). JMC thanks the CNRS-INSU Programme National de Planétologie for their support. We acknowledge Chris Rippon (Barberton Mines (Pty) Limited) for providing sample material.

References

Agangi A, Hofmann A, Przybyłowicz W (2014) Trace element zoning of sulfides and quartz at Sheba and Fairview gold mines: clues to Mesoarchean mineralisation in the Barberton Greenstone Belt, South Africa. Ore Geol Rev 56:94–114

Agangi A, Przybyłowicz W, Hofmann A (2015) Trace element mapping of pyrite from Archean gold deposits—A comparison between PIXE and EPMA. Nucl Instrum Methods Phys Res, Sect B 348:302–306

Agangi A, Hofmann A, Eickmann B, Marin-Carbonne J, Reddy SM (2016) An atmospheric source of S in Mesoarchaean structurally-controlled gold mineralisation of the Barberton Greenstone Belt. Precambr Res 285:10–20

Altigani MAH, Merkle RKW, Dixon RD (2016) Geochemical identification of episodes of gold mineralisation in the Barberton Greenstone Belt, South Africa. Ore Geol Rev 75:186–205

Anhaeusser CR (1976) Archean metallogeny in southern Africa. Econ Geol 71:16–43

Anhaeusser CR (1984) Structural elements of Archaean granite-greenstone terranes as exemplified by the Barberton Mountain Land, Southern Africa. In: Kröner A, Greiling R (eds) Precambrian Tectonics Illustrated. E. Schweizerbart'sche Verlagsbuchhandlung, Stuttgart, pp 57–58

Anhaeusser CR (1986) Archaean gold mineralization in the Barberton Mountain Land. In: Anhaeusser CR, Maske S (eds) Mineral

deposits of southern Africa, Geological Society of South Africa, pp 113–154
Anhaeusser CR (2001) The anatomy of an extrusive-intrusive Archaean mafic-ultramafic sequence: the Nelshoogte Schist Belt and Stolzburg Layered Ultramafic Complex, Barberton Greenstone Belt, South Africa. S Afr J Geol 104:167–204
Armstrong RA, Compston W, Retief EA, Williams IS, Welke HJ (1991) Zircon ion microprobe studies bearing on the age and evolution of the Witwatersrand triad. Precambr Res 53:243–266
Bao H, Rumble D III, Lowe DR (2007) The five stable isotope compositions of Fig Tree barites: implications on sulfur cycle in ca. 3.2-Ga oceans. Geochimica et Cosmochimica Acta 71:4868–4879
Barberton Gold Mines (2010) Mineral resources and technical short form report. www.panafricanresources.com. Consulted Nov 2012
Barberton Gold Mines (2014) Mineral resources and mineral reserve report. www.panafricanresources.com. Consulted Feb 2017
Bath AB, Walshe JL, Cloutier J, Verrall M, Cleverley JS, Pownceby MI, Macrae CM, Wilson NC, Tunjic J, Nortje GS, Robinson P (2013) Biotite and apatite as tools for tracking pathways of oxidized fluids in the Archean East Repulse gold deposit, Australia. Econ Geol 108:667–690
Cabri LJ, Chryssoulis SL, de Villiers JPR, Laflamme JHG, Buseck PR (1989) The nature of "invisible" gold in arsenopyrite. The Canadian Mineralogist 27:353–362
Cutts KA, Stevens G, Hoffmann JE, Buick IS, Frei D, Münker C (2014) Paleo- to Mesoarchean polymetamorphism in the Barberton Granite-Greenstone Belt, South Africa: Constraints from U-Pb monazite and Lu-Hf garnet geochronology on the tectonic processes that shaped the belt. Geol Soc Am Bull 126:251–270
de Boorder H (2012) Spatial and temporal distribution of the orogenic gold deposits in the late Palaeozoic Variscides and Southern Tianshan: how orogenic are they? Ore Geol Rev 46:1–31
de Ronde CEJ, de Wit MJ (1994) Tectonic history of the Barberton greenstone belt, South Africa: 490 million years of Archean crustal evolution. Tectonics 13:983–1005
de Ronde CEJ, Kamo SL (2000) An Archaean arc-arc collisional event: a short-lived (ca 3 Myr) episode, Weltevreden area, Barberton greenstone belt, South Africa. J Afr Earth Sc 30:219–248
de Ronde CEJ, Kamo S, Davis DW, de Wit MJ, Spooner ETC (1991) Field, geochemical and U-Pb isotopic constraints from hypabyssal felsic intrusions within the Barberton greenstone belt, South Africa: implications for tectonics and the timing of gold mineralization. Precambr Res 49:261–280
de Ronde CEJ, Spooner ETC, de Wit MJ, Bray CJ (1992) Shear zone-related, Au quartz vein deposits in the Barberton greenstone belt, South Africa; field and petrographic characteristics, fluid properties, and light stable isotope geochemistry. Econ Geol 87:366–402
Diener JFA, Stevens G, Kisters AFM, Poujol M (2005) Metamorphism and exhumation of the basal parts of the Barberton greenstone belt, South Africa: constraining the rates of Mesoarchaean tectonism. Precambr Res 143:87–112
Dirks PHGM, Charlesworth EG, Munyai MR (2009) Cratonic extension and Archaean gold mineralisation in the Sheba-Fairview mine, Barberton greenstone belt, South Africa. S Afr J Geol 112:291–316
Dirks PHGM, Charlesworth EG, Munyai MR, Wormald R (2013) Stress analysis, post-orogenic extension and 3.01 Ga gold mineralisation in the Barberton Greenstone Belt, South Africa. Precambrian Res 226:157–184
Doublier MP, Thébaud N, Wingate MTD, Romano SS, Kirkland CL, Gessner K, Mole DR, Evans N (2014) Structure and timing of Neoarchean gold mineralization in the Southern Cross district (Yilgarn Craton, Western Australia) suggest leading role of late Low-Ca I-type granite intrusions. J Struct Geol 67, Part B: 205–221
Drabon N, Lowe DR, Byerly G, Harrington JA (2017) Detrital zircon geochronology of sandstones of the 3.6–3.2 Ga Barberton greenstone belt: no evidence for older continental crust. Geology 45:803–806
Dziggel A, Kisters AFM (2019) Chapter 26—Tectono-metamorphic controls on Archean gold mineralization in the Barberton Greenstone Belt, South Africa. In: Van Kranendonk RH, Bennet VC Hoffmann E (eds) Earth's oldest rocks 2nd Ed, Elsevier, pp 655–674
Dziggel A, Stevens G, Poujol M, Anhaeusser CR, Armstrong RA (2002) Metamorphism of the granite-greenstone terrane south of the Barberton greenstone belt, South Africa: an insight into the tectono-thermal evolution of the lower portions of the Onverwacht Group. Precambr Res 114:221–247
Dziggel A, Armstrong RA, Stevens G, Nasdala L (2005) Growth of zircon and titanite during metamorphism in the granitoid-gneiss terrane south of the Barberton greenstone belt, South Africa. Mineral Mag 69:1019–1036
Dziggel A, Knipfer S, Kisters AFM, Meyer FM (2006) P-T and structural evolution during exhumation of high-T, medium-P basement rocks in the Barberton Mountain Land, South Africa. J Metamorph Geol 24:535–551
Dziggel A, Otto A, Kisters AFM, Meyer FM (2007) Chapter 5.8 Tectono-metamorphic controls on Archean gold mineralization in the Barberton Greenstone Belt, South Africa: an example from the New Consort gold mine. In: Van Kranendonk, MJ, Smithies, RH & Bennet, VC (eds) Earth's oldest rocks, Elsevier, Amsterdam, pp 699–727
Dziggel A, Poujol M, Otto A, Kisters AFM, Trieloff M, Schwarz WH, Meyer FM (2010) New U-Pb and $^{40}Ar/^{39}Ar$ ages from the northern margin of the Barberton greenstone belt, South Africa: implications for the formation of Mesoarchaean gold deposits. Precambr Res 179:206–220
Farquhar J, Bao H, Thiemens M (2000) Atmospheric influence of Earth's earliest sulfur cycle. Science 289:756–758
Fougerouse D, Micklethwaite S, Ulrich S, Miller J, Godel B, Adams DT, McCuaig TC (2016) Evidence for two stages of mineralisation in west Africa's largest gold deposit: Obuasi, Ghana. Econ Geol 112:2–33
Frimmel HE, Groves DI, Kirk J, Ruiz J, Chesley J, Minter WEL (2005) The formation and preservation of the Witwatersrand goldfields, the world's largest gold province. Econ Geol 100th Anniversary Volume:769–698
Fu B, Touret JLR (2014) From granulite fluids to quartz-carbonate megashear zones: the gold rush. Geosci Front 5:747–758
Gaboury D (2013) Does gold in orogenic deposits come from pyrite in deeply buried carbon-rich sediments?: insight from volatiles in fluid inclusions. Geology 41:1207–1210
Goldfarb RJ, Groves DI (2015) Orogenic gold: common or evolving fluid and metal sources through time. Lithos 233:2–26
Grosch EG, McLoughlin N (2013) Paleoarchean sulfur cycle and biogeochemical surface conditions on the early Earth, Barberton, South Africa. Earth Planet Sci Lett 377–378:142–154
Groves DI, Goldfarb RJ, Knox-Robinson CM, Ojala J, Gardoll S, Yun GY, Holyland P (2000) Late-kinematic timing of orogenic gold deposits and significance for computer-based exploration techniques with emphasis on the Yilgarn Block, Western Australia. Ore Geol Rev 17:1–38
Groves DI, Goldfarb RJ, Robert F, Hart CJR (2003) Gold deposits in metamorphic belts: overview of current understanding, outstanding problems, future research, and exploration significance. Econ Geol 98:1–29
Harris PD, Robb LJ, Tomkinson MJ (1995) The nature and structural setting of rare-element pegmatites along the northern flank of the Barberton greenstone belt, South Africa. S Afr J Geol 98:82–94
Hazarika P, Mishra B, Pruseth KL (2017) Trace-element geochemistry of pyrite and arsenopyrite: ore genetic implications for late Archean orogenic gold deposits in southern India. Mineral Mag 81:661

Hegner E, Kröner A, Hofmann AW (1984) Age and isotope geochemistry of the Archaean Pongola and Usushwana suites in Swaziland, Southern Africa: a case for crustal contamination of mantle-derived magma. Earth Planet Sci Lett 70:267–279

Heubeck C, Engelhardt J, Byerly GR, Zeh A, Sell B, Luber T, Lowe DR (2013) Timing of deposition and deformation of the Moodies Group (Barberton Greenstone Belt, South Africa): very-high-resolution of Archaean surface processes. Precambr Res 231:236–262

Heubeck C, Bläsing S, Grund M, Drabon N, Homann M, Nabhan S (2016) Geological constraints on Archean (3.22 Ga) coastal-zone processes from the Dycedale Syncline, Barberton greenstone belt. S Afr J Geol 119:495

Hofmann A (2005) The geochemistry of sedimentary rocks from the Fig Tree Group, Barberton greenstone belt: implications for tectonic, hydrothermal and surface processes during mid-Archaean times. Precambr Res 143:23–49

Hofmann A, Pitcairn I, Wilson A (2017) Gold mobility during Palaeoarchaean submarine alteration. Earth Planet Sci Lett 462:47–54

Hronsky J, Groves D, Loucks R, Begg G (2012) A unified model for gold mineralisation in accretionary orogens and implications for regional-scale exploration targeting methods. Miner Deposita 47:339–358

Johnston DT (2011) Multiple sulfur isotopes and the evolution of Earth's surface sulfur cycle. Earth Sci Rev 106:161–183

Kakegawa T, Ohmoto H (1999) Sulfur isotope evidence for the origin of 3.4 to 3.1 Ga pyrite at the Princeton gold mine, Barberton greenstone belt, South Africa. Precambr Res 96:209–224

Kamo SL, Davis DW (1994) Reassessment of Archean crustal development in the Barberton Mountain Land, South Africa, based on U-Pb dating. Tectonics 13:167–192

Kendrick MA, Honda M, Walshe J, Petersen K (2011) Fluid sources and the role of abiogenic-CH_4 in Archean gold mineralization: Constraints from noble gases and halogens. Precambr Res 189(3–4):313–327

Kirk J, Ruiz J, Chesley J, Walshe J, England G (2002) A major Archean, gold- and crust-forming event in the Kaapvaal Craton, South Africa. Science 297:1856–1858

Kisters AFM, Stevens G, Dziggel A, Armstrong RA (2003) Extensional detachment faulting and core-complex formation in the southern Barberton granite-greenstone terrain, South Africa: evidence for a 3.2 Ga orogenic collapse. Precambr Res 127:355–378

Kisters AFM, Belcher RW, Poujol M, Dziggel A (2010) Continental growth and convergence-related arc plutonism in the Mesoarchaean: evidence from the Barberton granitoid-greenstone terrain, South Africa. Precambr Res 178:15–26

Kolb J, Dziggel A, Bagas L (2015) Hypozonal lode gold deposits: a genetic concept based on a review of the New Consort, Renco, Hutti, Hira Buddini, Navachab, Nevoria and the granites deposits. Precambr Res 262:20–44

Kositcin N, Krapez B (2004) Relationship between detrital zircon age-spectra and the tectonic evolution of the late Archaean Witwatersrand Basin, South Africa. Precambr Res 129:141–168

Kröner A, Hegner E, Wendt JI, Byerly GR (1996) The oldest part of the Barberton granitoid-greenstone terrain, South Africa: evidence for crust formation between 3.5 and 3.7 Ga. Precambr Res 78:105–124

Kröner A, Anhaeusser CR, Hoffmann JE, Wong J, Geng H, Hegner E, Xie H, Yang J, Liu D (2016) Chronology of the oldest supracrustal sequences in the Palaeoarchaean Barberton Greenstone Belt, South Africa and Swaziland. Precambr Res 279:123–143

Lana C, Tohver E, Cawood P (2010) Quantifying rates of dome-and-keel formation in the Barberton granitoid-greenstone belt, South Africa. Precambr Res 177:199–211

Lowe DR (1999) Geologic evolution of the Barberton Greenstone Belt and vicinity. Geological Society of America Special Papers 329:287–312

Lowe DR, Byerly GR (1999) Stratigraphy of the west-central part of the Barberton Greenstone Belt, South Africa. Geological Society of America Special Papers 329:1–36

Lowe DR, Byerly GR (2007) An overview of the geology of the Barberton Greenstone Belt and vicinity: implications for early crustal development. In: Van Kranendonk MJ, Smithies RH, Bennett VC (eds) Earth's oldest rocks. Elsevier, Amsterdam, pp 481–524

Lowe, DR, Byerly, GR, Heubeck, C (2012) Geologic Map of the west-central Barberton greenstone belt. In: South Africa, scale 1:25,000: Geological Society of America Map and Chart Series No. 103

Maphalala R, Kröner A (1993) Pb-Pb single zircon ages for the younger Archaean granitoids of Swaziland, southern Africa. In: Maphalala R, Mabuza M (eds) 16th Colloquium of African Geology. Swaziland Geological Survey and Mines 2: 201–206

Matsumura R (2014) The petrogenesis of the Nelshoogte pluton: the youngest and most compositionally variable TTG pluton in the Barberton Granite-Greenstone Terrain. Unpublished MSc thesis, Stellenbosch University, 108 p

Mishra B, Pruseth KL, Hazarika P, Chinnasamy SS (2017) Nature and source of the ore-forming fluids associated with orogenic gold deposits in the Dharwar Craton. Geosci Front 9:715–726

Montinaro A, Strauss H, Mason PRD, Roerdink D, Münker C, Schwarz-Schampera U, Arndt NT, Farquhar J, Beukes NJ, Gutzmer J, Peters M (2015) Paleoarchean sulfur cycling: multiple sulfur isotope constraints from the Barberton greenstone belt, South Africa. Precambr Res 267:311–322

Morey AA, Tomkins AG, Bierlein FP, Weinberg RF, Davidson GJ (2008) Bimodal distribution of gold in pyrite and arsenopyrite: examples from the Archean Boorara and Bardoc shear systems, Yilgarn Craton, Western Australia. Econ Geol 103:599–614

Moyen J-F, Stevens G, Kisters A (2006) Record of mid-Archaean subduction from metamorphism in the Barberton terrain, South Africa. Nature 442:559–562

Munyai MR, Dirks PHGM, Charlesworth EG (2011) Archaean gold mineralisation during post-orogenic extension in the New Consort gold mine, Barberton greenstone belt, South Africa. S Afr J Geol 114:121–144

Murphy RCL (2015) Stabilising a craton: the origin and emplacement of the 3.1 Ga Mpuluzi Batholith. Unpublished PhD thesis, Macquarie University, Sydney, Australia, 489p

Ono S, Eigenbrode JL, Pavlov AA, Kharecha P, Rumble D III, Kasting JF, Freeman KH (2003) New insights into Archean sulfur cycle from mass-independent sulfur isotope records from the Hamersley Basin, Australia. Earth Planet Sci Lett 213:15–30

Otto A, Dziggel A, Kisters A, Meyer F (2007) The New Consort Gold Mine, Barberton greenstone belt, South Africa: orogenic gold mineralization in a condensed metamorphic profile. Miner Deposita 42:715–735

Pearton T, Viljoen M (2017) Gold on the Kaapvaal Craton, outside the Witwatersrand Basin, South Africa. S Afr J Geol 120:101–132

Philippot P, van Zuilen M, Rollion-Bard C (2012) Variations in atmospheric sulphur chemistry on early Earth linked to volcanic activity. Nat Geosci 5:668–674

Phillips GN, Powell R (2009) Formation of gold deposits: review and evaluation of the continuum model. Earth Sci Rev 94:1–21

Pokrovski GS, Akinfiev NN, Borisova AY, Zotov AV, Kouzmanov K (2014) Gold speciation and transport in geological fluids: insights from experiments and physical-chemical modelling. Geol Soc Spec Pub 402:9–70

Poujol M, Robb LJ, Respaut J-P, Anhaeusser CR (1996) 3.07–2.97 Ga greenstone belt formation in the northeastern Kaapvaal Craton; implications for the origin of the Witwatersrand Basin. Econ Geol 91:1455–1461

Qiu Y, McNaughton NJ (1999) Source of Pb in orogenic lode-gold mineralisation: Pb isotope constraints from deep crustal rocks from the southwestern Archaean Yilgarn Craton, Australia. Mineralium Deposita 34(4):366–381

Reich M, Kesler SE, Utsunomiya S, Palenik CS, Chryssoulis SL, Ewing RC (2005) Solubility of gold in arsenian pyrite. Geochimica et Cosmochimica Acta 69:2781–2796

Roerdink DL, Mason PRD, Farquhar J, Reimer T (2012) Multiple sulfur isotopes in Paleoarchean barites identify an important role for microbial sulfate reduction in the early marine environment. Earth Planet Sci Lett 331–332:177–186

Roerdink DL, Mason PRD, Whitehouse MJ, Reimer T (2013) High-resolution quadruple sulfur isotope analyses of 3.2 Ga pyrite from the Barberton Greenstone Belt in South Africa reveal distinct environmental controls on sulfide isotopic arrays. Geochimica et Cosmochimica Acta 117:203–215

SACS (1980) Stratigraphy of South Africa Part 1: Lithostratigraphy of the Republic of South Africa, South West Africa/Namibia and the Republics of Bophuthatswana, Transkei and Venda. Geological Survey of South Africa, 690p

Sahoo PR, Venkatesh AS (2015) Constraints of mineralogical characterization of gold ore: implication for genesis, controls and evolution of gold from Kundarkocha gold deposit, eastern India. J Asian Earth Sci 97, Part A: 136–149

Salier BP, Groves DI, McNaughton NJ, Fletcher IR (2005) Geochronological and stable isotope evidence for widespread orogenic gold mineralization from a deep-seated fluid source at ca 2.65 Ga in the Laverton Gold Province, Western Australia. Econ Geol 100:1363–1388

Schoene B, de Wit MJ, Bowring SA (2008) Mesoarchean assembly and stabilization of the eastern Kaapvaal craton: a structural-thermochronological perspective. Tectonics 27:TC5010

Schouwstra RP (1995) Wall-rock alteration as a guide to gold-bearing fracture zones in the Zwartkoppie Section, Sheba gold mine, South Africa. S Afr J Geol 98:399–414

Schouwstra RP, De Villier J (1998) Gold mineralization and associated wallrock alteration in the Main Reef Complex at Sheba Mine, South Africa. Appl Earth Sci IMM Trans Sect B:B158–B170

Selvaraja V, Fiorentini ML, Jeon H, Savard DD, LaFlamme CK, Guagliardo P, Caruso S, Bui T-H (2017) Evidence of local sourcing of sulfur and gold in an Archaean sediment-hosted gold deposit. Ore Geol Rev 89:909–930

Sibson RH, Robert F, Poulsen KH (1988) High-angle reverse faults, fluid-pressure cycling, and mesothermal gold-quartz deposits. Geology 16:551–555

Stiegler MT, Cooper M, Byerly GR, Lowe DR (2012) Geochemistry and petrology of komatiites of the pioneer ultramafic complex of the 3.3 Ga Weltevreden formation, Barberton greenstone belt, South Africa. Precambr Res 212:1–12

Tomkins AG (2013) On the source of orogenic gold. Geology 41:1255–1256

Van Kranendonk MJ, Kröner A, Hegner E, Connelly J (2009) Age, lithology and structural evolution of the c. 3.53 Ga Theespruit Formation in the Tjakastad area, southwestern Barberton greenstone belt, South Africa, with implications for Archaean tectonics. Chem Geol 261:115–139

Viljoen MJ, Viljoen RP (1969) Introduction to the geology of the Barberton granite-greenstone terrain. Geological Society of South Africa Special Publication 2:9–28

Wang LG, McNaughton NJ, Groves DI (1993) An overview of the relationship between granitoid intrusions and gold mineralisation in the Archaean Murchison Province, Western Australia. Mineralium Deposita 28(6):482–494

Ward JHW (1995) Geology and metallogeny of the Barberton greenstone belt: a survey. J Afr Earth Sc 21:213–240

Ward JHW (1999) The metallogeny of the Barberton greenstone belt, South Africa and Swaziland. Geological Survey of South Africa Memoir 86, 108p

Wilson AH, Zeh A (2019) U-Pb and Hf isotopes of detrital zircons from the Pongola Supergroup: constraints on deposition ages, provenance and Archean evolution of the Kaapvaal craton. Precambrian Research 305 (Supplement C): 177–196

Wit De et al (2019) Paleoarchean bedrock lithologies across the Makhonjwa Mountains of South Africa and Swaziland linked to geochemical, magnetic and tectonic data reveal early plate tectonic genes flanking subduction margins. Geosci Front 9:603–665

Zeh A, Gerdes A, Heubeck C (2013) U-Pb and Hf isotope data of detrital zircons from the Barberton greenstone belt: constraints on provenance and Archaean crustal evolution. J Geol Soc 170:215–223